Journal of Interfaces, Thin films, and Low dimensional systems 5 (2) Winter and Spring (2022) 493-503

Linear optical modeling on aluminum zig-zag thin films

Scientific research paper

Mahsa Fakharpour[1*], Maryam Gholizadeh Arashti[2]

Department of Physics, Maybod Branch, Islamic Azad University, Maybod, Iran

Department of Physics, Yadegar-e-Imam Khomeini (RAH) Shahre Rey Branch, Islamic Azad University, Tehran, Iran

ARTICLE INFO

Article history:
Received 22 September 2022
Revised 20 February 2023
Accepted 12 March 2023
Available online 14 April 2023

Keywords
Reflectance
Transfer matrix
Zig-zag nanostructure
Linearly polarized light
Bragg phenomenon

ABSTRACT

The Al zig-zag sculptured thin film consists of two identical columns, the first nanocolumns (zig) are oriented at the angle χ and the second nanocolumns (zag) are oriented at the angle $(\pi- \chi)$. The optical properties of these nanostructures were obtained using the transfer matrix method for linear s- and p- polarized incident lights in the wavelength range of 300-1000 nm. The reflection and transmission spectra of the zig-zag nanostructures with different arm numbers and lengths were obtained at different incident angles. The Bragg peaks begin to appear for zig-zag nanostructures of more than 4 arms for s- polarized light at the angles greater than 30°. For zig-zag structures of 4, 8, and 16 arms, one, two, and three Bragg peaks were observed, respectively. However, for p- polarized light, no Bragg peak was observed at any of the incident angles. Also, for the zig-zag structure of 8 arms for s-polarized light at 60° incident angles, the number of Bragg peaks increases with increasing the arm length. In addition, the peaks created in the wavelengths below 550 nm showed red shift while the peaks appeared in the wavelengths above 550 nm showed blue shift.

1 Introduction

In the recent years, the metal-dielectric composite layers have been increasingly regarded and their structural, optical and electrical properties have been widely studied, both experimentally and theoretically. Among the metallic elements used in these composite layers, aluminum (Al) has received special attention due to its simple thin film preparation process [1, 2]. The electrical conductivity near its bulk value [3] also introduces an ideal element for the optoelectronic devices production [4, 5]. The physical properties of Al thin films sensitively relate to their microstructures [6, 7], so it may be manipulated [8-10] controllably. The plasmonic properties of $Al@Al_2O_3$, suggests it as a suitable candidate for tremendous applications due to wide ranges of plasmonic resonances from deep UV to the middle visible region [11].

The glancing angle deposition (GLAD) and oblique angle deposition (OAD) methods are usual to make porous thin films with controlled nanostructures. Non-isotropic structure of porous thin films [12, 13] causes tensional anisotropy and optical birefringence [14] and also affects their magnetic permeability [15]. The anisotropic degree relates to the element and substrate types and

*Corresponding author.
Email address: Mahsafakharpour@Yahoo.com
DOI: 10.22051/jitl.2023.42264.1076

deposition angle [16]. Optically anisotropic thin films have a variety of applications including speed reduction optical plates [17], anisotropic antireflection coating [18], birefringent omnidirectional reflector [19], 3D photonic band gap crystals [20], birefringent thin film polarizers [21], new optical filters [14], polarization-selective and Bragg mirrors and interferential filters [22]. Porous thin films were prepared with different structural properties, frequency filtering abilities and desired geometric shapes such as chiral, zig-zag and nano flowers, and studied under the s- and p- polarized light irradiations [23-29].

RahChamani et al. prepared zig-zag nano-sculptured ZnS thin films by the GLAD technique and showed that their refractive indexes are highly sensitive to the preparation conditions [23]. They also studied the optical properties of zig-zag nano-sculptured ZnS thin films with different growth angles at 10° and 70° incident light angles for both s- and p-polarized lights and showed their significant difference, indicating the employed angles were above the Brewster's angle of ZnS film [24]. Liedtke et al. showed that the porosity significantly influences the incident angle and substrate temperature [25]. There are many other issues on zig-zag thin film preparation by different methods [26-29].

The Bragg reflection is a phenomenon for creation of controllable optical filter components. A variety of theoretical methods have been used to study the optical properties of porous thin films. The transition matrix is a useful method to determine the optical properties of anisotropic thin films by different morphologies. In this method, the structure of porous metal composite homogenizes the Bruggeman formula to obtain the effective dielectric properties of the layers [30, 31]. The material-void fraction, material local direction and the layer thickness are the main parameters needed for the homogenization. Reduction of the electrical field amplitude in the anisotropic composite materials and high real scaler values of the metals electric permeability makes difficulties in the calculation of the reflection and transmission amplitudes, even for thick layers. To overcome these difficulties, the anisotropic material is usually considered as a semi-space structure to obtain its reflection for vertical incident light [20].

Vepachedu et al. [32] fabricated Chevronic and Zigzag (Bragg mirror) sculptured thin films of ZnSe with N = 10 unit cells. The Bragg phenomenon of order m=2 for Bragg mirror thin film was observed at θ=ψ=0° and ψ=90° (incident angle θ and azimuthal angle ψ), and the Chevronic sculptured thin film (with the same arms lengths and 20° growth angle) did not exhibit the Bragg phenomenon. Their theoretical results for zigzag thin film of TiO_2 with N=30 unit cells showed the Bragg phenomenon of order m=2,3 at ψ=θ=0°, while this phenomenon was observed in Chevronic thin film of TiO_2 for highly oblique incidence.

This work is devoted to the study of linearly polarized light propagation in the Al zig-zag thin films, using transfer matrix method. At first, the Bragg phenomena of Al zig-zag thin films were simulated and studied for both s- and p- polarized incident light for different number of arms and incident light angles. The effects of nanostructure arm lengths on the Bragg phenomena were also investigated.

2 Optical modelling

The harmonic time dependency of the incident light is considered as $\exp(i\omega t)$ which ω shows the angular frequency. The wave number, wavelength, and intrinsic impedance of free space are denoted by $k = \omega\sqrt{\varepsilon_0\mu_0}$, $\lambda = 2\pi/k$ and $\eta_0 = \sqrt{\varepsilon_0/\mu_0}$, respectively. μ_0 and ε_0 show the magnetic permeability and electrical permittivity of the free space, respectively. The Cartesian unit vectors are displayed by $\underline{u}_x$, $\underline{u}_y$, and $\underline{u}_z$ The vectors are underlined once and the dyadic is underlined twice.

The studied model structure is a zig-zag thin film occupied in the region $0 \le z \le d$ surrounded by vacuous regions $z < 0$ and $z > d$ as given in Fig. 1.

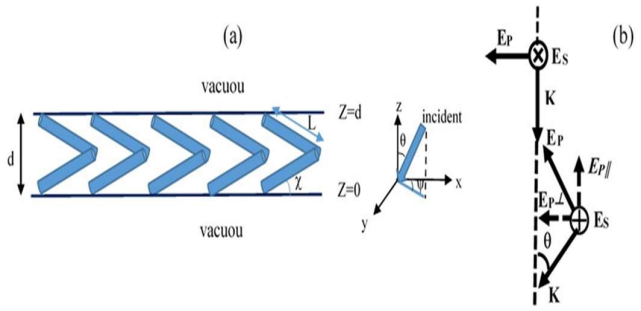

Figure 1. Schematic representation of the modeled zig-zag thin film.

The relative permittivity dyadic $\underline{\underline{\varepsilon}}(z,\omega)$ is nonhomogeneous denoted by:

$$\begin{cases} \underline{\underline{\varepsilon}}(z,\omega) = \underline{\underline{S_z}}(\zeta).\underline{\underline{S_y}}(\chi).\underline{\underline{\varepsilon_{ref}}}(\omega).\underline{\underline{S_y^T}}(\chi)\underline{\underline{S_z^T}}(\zeta) \\ \underline{\underline{\varepsilon_{ref}}}(\omega) = \varepsilon_a(\omega)\underline{\underline{I}} + \left[\varepsilon_b(\omega) - \varepsilon_a(\omega)\right] u_x u_x \end{cases}, \quad (1)$$

Where $\underline{\underline{\varepsilon_{ref}}}(\omega)$ is a reference relative permittivity dyadic; $\varepsilon_a(\omega)$ and $\varepsilon_b(\omega)$ are the material and void; $\underline{\underline{I}} = u_x u_x + u_y u_y + u_z u_z$ is the identity dyadic; and the superscript ^{T} denotes the transpose. $\underline{\underline{S_z}}(\zeta)$ and $\underline{\underline{S_y}}(\chi)$ indicated rotation dyadics about the z and y axis. ζ and χ are the rotation angle of the arms about z-axis and the growth angle of columns to xy-plane, respectively. It is assumed that the structure is excited by a plane wave propagating with the incident angle θ to the z-axis and azimuthal angle ψ with the x-axis in the xy-plane. The phasors of incident, reflected, and transmitted electric fields are given by [20]

$$\begin{cases} \underline{E}_{inc} = (a_s \underline{s} + a_p \underline{p}_+) e^{ik_0 z\cos\theta} \exp(i(kx\cos\psi + ky\sin\psi)) & z \le 0 \\ \underline{E}_{ref} = (r_s \underline{s} + r_p \underline{p}_-) e^{-ik_0 z\cos\theta} \exp(i(kx\cos\psi + ky\sin\psi)) & z \le 0 \\ \underline{E}_{tr} = (t_s \underline{s} + t_p \underline{p}_+) e^{ik_0 (z-L)\cos\theta} \exp(i(kx\cos\psi + ky\sin\psi)) & z \ge d \end{cases}, (2)$$

that is expressed in terms of the s- and p- polarized light components via the unit vectors

$$\begin{cases} \underline{s} = -\underline{u}_x \sin\psi + \underline{u}_y \cos\psi \\ \underline{p}_\pm = \mp(\underline{u}_x \cos\psi + \underline{u}_y \sin\psi)\cos\theta + \underline{u}_z \sin\theta \end{cases}. (3)$$

The parameters (a_s, a_p), (r_s, r_p) and (t_s, t_p) show the amplitudes of incident, reflected, and transmitted waves, respectively with the s- and p- indexes as the linear polarization types. The phasor of the magnetic field in any region is given by $\underline{H} = (i\omega\mu_0)^{-1}\underline{\nabla} \times \underline{E}$. We also have the following equations in the Cartesian coordinate system

$$\begin{cases} \underline{r} = x\underline{u}_x + y\underline{u}_y + z\underline{u}_z \\ \underline{k}_0 = k_0\left(\sin\theta\cos\psi\,\underline{u}_x + \sin\theta\sin\psi\,\underline{u}_y + \cos\theta\,\underline{u}_z\right) \end{cases}. (4)$$

The continuity of the tangential components of the electrical and magnetic fields at the interfaces of thin films may be used to calculate the reflectance and transmittance amplitudes through the solution of the algebraic matrix equation:

$$\begin{bmatrix} t_s \\ t_p \\ 0 \\ 0 \end{bmatrix} = \left[\underline{\underline{K}}(\theta,\psi)\right]^{-1}.\left[\underline{\underline{M}}(d,k,\psi)\right].\left[\underline{\underline{K}}(\theta,\psi)\right].\begin{bmatrix} a_s \\ a_p \\ r_s \\ r_p \end{bmatrix}, (5)$$

The different terms and parameters of this equation are described in details, in reference [20].

We now consider a zig-zag thin film with thickness of $d = Nt_z$, where t_z is the thickness of an arm of zig-zag, and N is the number of arms. The transfer matrix of a columnar thin film with thickness of d is given by $e^{i\left[\underline{\underline{P}}\right]t}$ [20]. Therefore, the transfer matrix of a zig-zag nanostructure is [23]

$$\left[\underline{\underline{M}}\right]_{zigzag} = \left[\underline{\underline{M}}\right]_N \left[\underline{\underline{M}}\right]_{N-1} \ldots \left[\underline{\underline{M}}\right]_2 \left[\underline{\underline{M}}\right]_d, \quad (6)$$

where $\left[\underline{\underline{M}}\right]_i = e^{i\left[\underline{\underline{P}}(\varsigma,\chi,\lambda_0,\theta,\psi)\right]t}$, $i = 1,2,\ldots,N$. Replacing $\left[\underline{\underline{M}}(d,k,\psi)\right]$ by the transfer matrix of zig-zag, $\left[\underline{\underline{M}}\right]_{zigzag}$ in Eq. (6), the reflectance and transmittance amplitudes may be calculated. The results in terms of the matrix relations, are

$$\begin{bmatrix} r_s \\ r_p \end{bmatrix} = \begin{bmatrix} r_{ss} & r_{sp} \\ r_{ps} & r_{pp} \end{bmatrix} \begin{bmatrix} a_s \\ a_p \end{bmatrix}, \quad (7)$$

and

$$\begin{bmatrix} t_s \\ t_p \end{bmatrix} = \begin{bmatrix} t_{ss} & t_{sp} \\ t_{ps} & t_{pp} \end{bmatrix} \begin{bmatrix} a_s \\ a_p \end{bmatrix}. \quad (8)$$

Four reflection r_{xy} and transmission t_{xy} coefficients with x and y in {s, p} were used to compute the

reflectances $R_{sp} = \left|r_{sp}\right|^2$, etc., and the transmittances $T_{sp} = \left|t_{sp}\right|^2$, etc., of the zig-zag thin film.

Thin film is wholly dissipative when the amplification is negligible. As a result, from the energy conservation principle, the inequalities must be hold

$$\begin{cases} R_{ss} + R_{ps} + T_{ss} + T_{ps} < 1 \\ R_{pp} + R_{sp} + T_{pp} + T_{sp} < 1 \end{cases}. \quad (9)$$

The optical absorption for s- and p-linear polarized lights are given by

$$A_i = 1 - \sum_{j=s,p} \left(R_{ji} + T_{ji}\right) \quad , \quad i = s, p \, . \quad (10)$$

In order to model the optical characteristics of the prepared sample, we have considered a zig-zag structure for which relative permittivity scalars $\varepsilon_{a,b,c}$ may be calculated using the Bruggeman homogenization equations [30]. In this formalism, the two- component structure is composed of the Al metal and void. The relative permittivity scalars depend to different parameters, including geometric form factor, fraction of Al (f_{Al}), the wavelength in the free space, and the refractive index. In addition, each column in the structure is considered as a string of identical long ellipsoids by small electrical interactions [30]. In all calculations, the columnar form factors are considered as

$$\left(\frac{c}{a}\right)_{Al} = \left(\frac{c}{a}\right)_{void} = 15, \quad \left(\frac{b}{a}\right)_{Al} = \left(\frac{b}{a}\right)_{void} = 1 \, , \quad (11)$$

that *c*, *a,* and *b* are semi major axis and small half axes of ellipsoids, respectively [33]. We have used the bulk experimental refractive index of Al for homogenization [34]. In homogenization of the structure, effects of dispersion and dissipation of the dielectric function are considered [35].

In order to investigate the optical properties of the Al zig-zag thin film, the growth angle of columns was considered χ=30° and the void fraction was fixed at 0.85. For metallic fraction greater than 0.2, it is very difficult to observe the Bragg phenomena [36]. Calculations were obtained using MATLAB software in the wavelength range of 300 to 1000 nm with a step of 5 nm and an accuracy of 0.1.

3. Results and discussion

3.1 Effect of the arms number

The co-remittance spectra (i.e., $R_{pp,\,ss}$ and $T_{pp,\,ss}$) of the Al zig-zag films with the arm numbers (2,4,8,16) at 0° azimuthal angle and the incident light angles 0°, 30°, 60° and 80° are plotted in Figs. 2 to 5 for both s and p-polarized incident lights. Since, the cross-reflection and transmission spectra are very small compared to those obtained for the co-remittance spectra, the cross-remittance spectra are ignored [37].

Figure 2 shows the co-reflection $R_{pp,\,ss}$ (Fig. 2a and 2b) and co-transmission $T_{pp,\,ss}$ (Fig. 2c and 2d) spectra for the Al zig-zag film with 2 arms at azimuthal angle ψ=0° and incident light angles θ = 0°, 30°, 60°. and 80° for both s and p- polarized lights. According to Figs. 2a and 2b, the co-reflection and co-transmission spectra for incident light angles θ = 0°, 30°, 60° and 80° for both s and p- polarized lights are opposite together. The Brewster angle of aluminum thin-film at wavelength of 667 nm is 82° [38]. Therefore, for s-polarized incident light, the intensity of co-reflection spectrum (Fig. 2b) increases with incident angle, while the co-transmission spectrum (Fig. 2d) decreases.

The intensity of the co-reflection (co-transmission) for s- polarized light increases (decreases) with the incident light angle (θ) from 0° to 80° that may be devoted to more interaction of the electric field (E_s) of the incident light with the structure surface. At azimuthal angles of 0°, the s- and p-polarized lights are perpendicular to each other, so the intensity of co-reflection (co-transmission) spectra for p-polarized light behaves opposite to the s-polarized light except at 80° that is near the Brewster angle. The intensity of co-reflection spectrum of p-polarized light decreases with the incident light angle, except at 80° that is near to the Brewster angle. Also, for the incident light angles 0° and 30°, three peaks can be observed at co-reflection spectrum of p- polarized light (R_{pp}) that shift towards lower wavelengths (blue shift), as the incident light angle increases. The behaviors of co-transmission spectrum of p- polarized light (T_{pp}) for different incident light angles are almost the same.

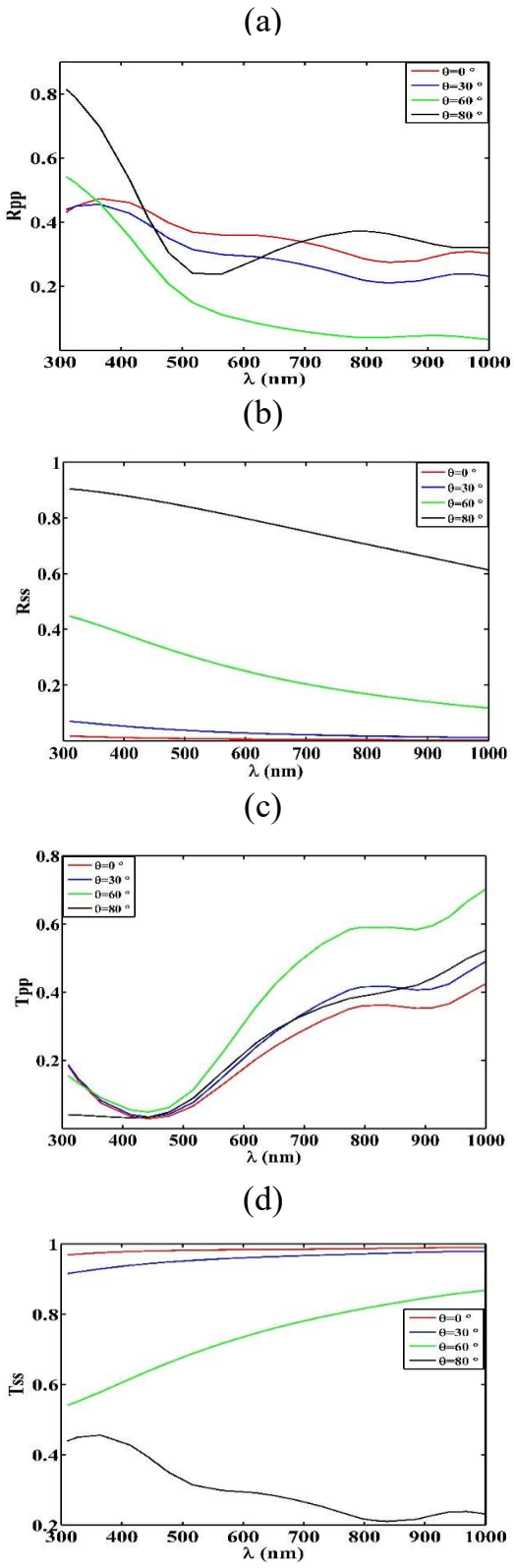

Figure 2. Co-polarized reflectances $R_{ss,\ pp}$ and co-polarized transmittances $T_{ss,\ pp}$ spectra for both s- and p- polarized lights at incident light angles (θ = 0°, 30°, 60° and 80°) and azimuthal angle ψ=0° for Al zig-zag thin films with two arms.

The co-remittance spectra (i.e., Rpp, ss and Tpp, ss) for the Al zig-zag film with 4 arms at the azimuthal angle 0° and the incident light angles 0°, 30°, 60°, and 80° for both s and p- polarized lights are shown in Fig. 3. As the incident light angle increases, the intensity of the co-reflection (co-transmission) for s-polarized incident light increases (decreases) (Fig. 3a and 3b). The reflection spectra (Fig. 3b) of the s-polarized incident light for 60° and 80° incident angles have very wide peaks at about 520 nm wavelength while transmission spectrum (Fig. 3d) has its minimum value. This may be considered as the beginning of the mirror Bragg phenomenon in these nanostructures. For the p-polarized incident light, and two arms, the behavior of transmission spectrum is the same at all incident angles. For the s-polarized incident light, as the incident light angle increases, except for the angles near the Brewster angle, the intensity of the co-reflection (co-transmission) decreases (increases). Also, in the reflection spectrum (R_{pp}) at 0° and 30° incident angles, a peak is created in the wavelengths greater than 1000 nm that is out of the assumed spectrum region. Increasing the incident angle to 60° and 80° creates a blue shift for the peak.

The co-remittance spectra (i.e., $R_{pp,\ ss}$ and $T_{pp,\ ss}$) for the Al zig-zag film with 8 arms (L=30 nm) at azimuthal angle 0° and incident light angles of 0°, 30°, 60° and 80° for both s and p- polarized lights are plotted in the Fig. 4. Increasing the incident light angle creates some peaks in the reflection spectrum of s- polarized incident light. In the reflection spectrum (Fig. 4b) for the incident angles 60° and 80°, two peaks may be clearly observed in λ = 364 nm and λ ≳900 nm for which the transmission spectrum (Fig. 4d) had decreased. In other words, the mirror Bragg phenomenon occurs at these wavelengths that become more obvious by increasing the incident light angle.

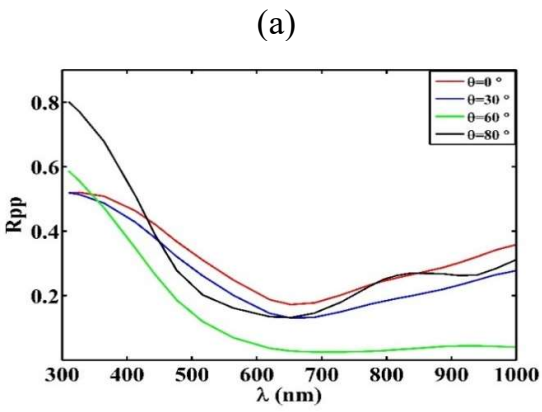

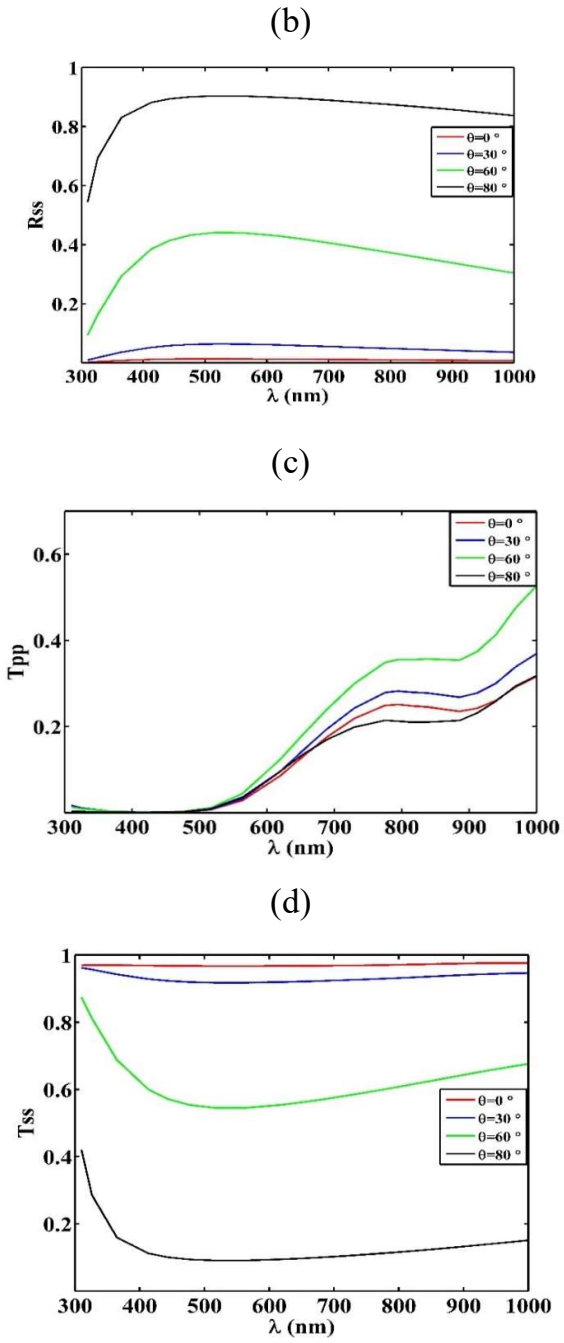

Figure 3. Co-polarized reflectances $R_{ss,\,pp}$ and transmittances $T_{ss,\,pp}$ spectra for s- and p- polarized lights at θ = 0°, 30°, 60° and 80° incident light angles and azimuthal angle ψ=0° for Al zig-zag thin film with four arms.

The behavior of co-remittance spectra for p- polarized incident light (i.e., R_{pp} and T_{pp}), are similar to the Al zig-zag film with 4 arms.

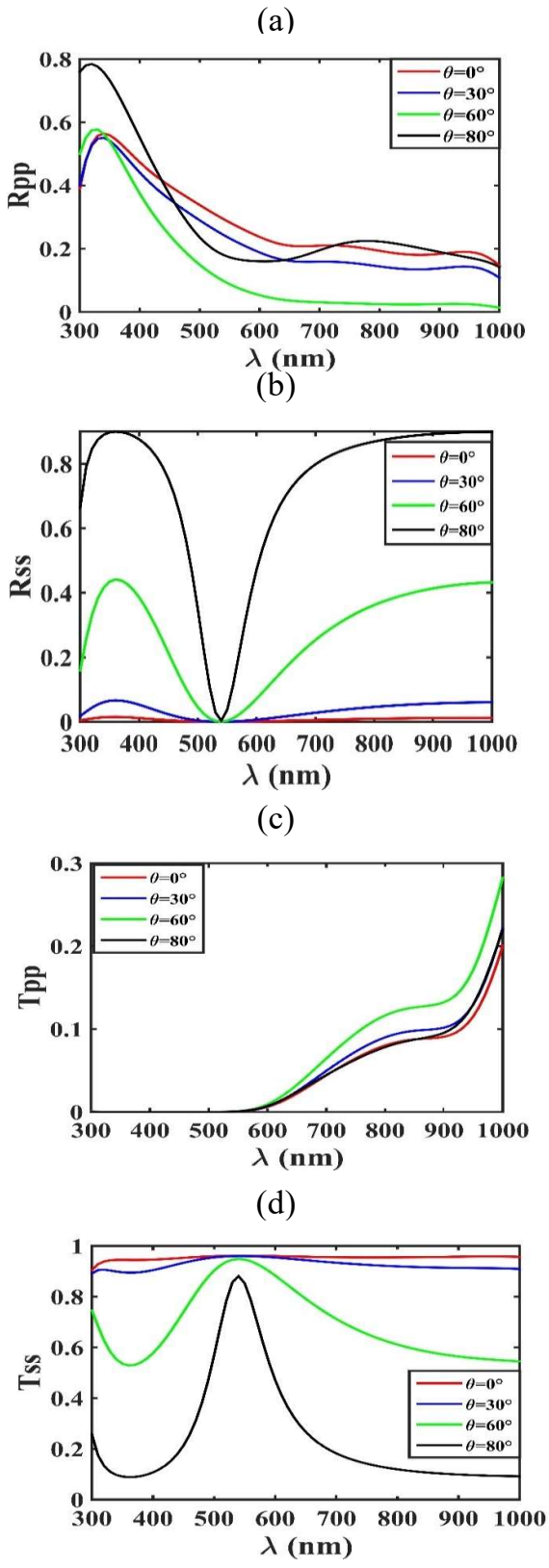

Figure 4. Co-polarized reflectances $R_{ss,\,pp}$ and co-polarized transmittances $T_{ss,\,pp}$ spectra for both s- and p- polarized lights for different incident light angles (θ = 0°, 30°, 60° and 80°) and azimuthal angle ψ=0° for Al zig-zag thin films with 8 arms.

The co-remittance spectra (i.e., $R_{pp,\ ss}$ and $T_{pp,\ ss}$) for the Al zig-zag film with 16 arms at azimuthal angle 0° and incident light angles 0°, 30°, 60°, and 80° for both s and p- polarized lights are shown in the figure 5. Three peaks can be seen at λ = 300 nm, λ = 427 nm and λ= 730 nm for s-polarized incident light for which the reflection spectra (Fig. 5b) are maximized and the transmission spectra (Fig. 5d) are reduced. As the incident light angle increases, the intensity of the mirror Bragg phenomenon increases, without any displacement of wavelengths. For the p- polarized incident light, as in the previous cases, no Bragg phenomenon was observed.

(a)

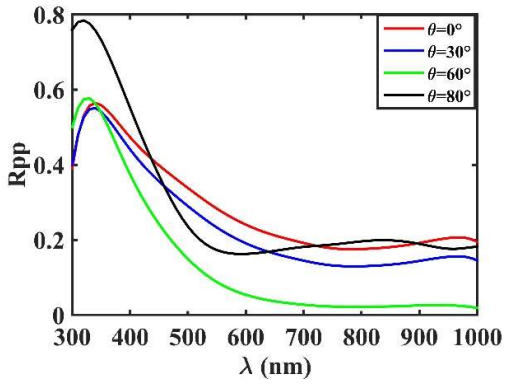

(b)

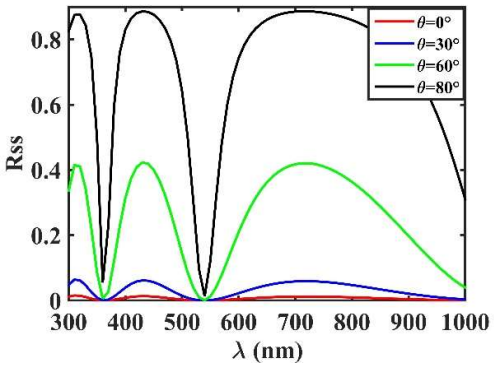

(c)

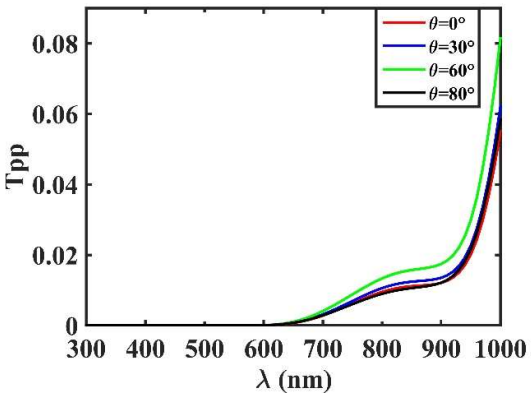

(d)

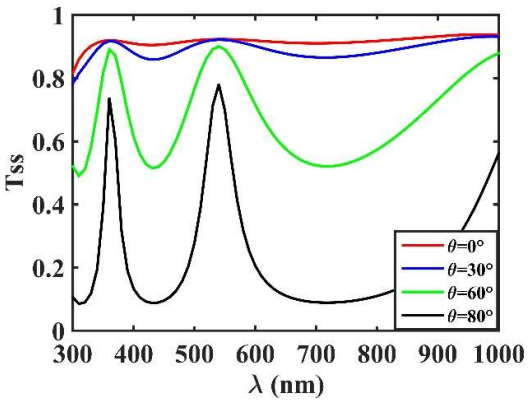

Figure 5. Co-polarized reflectance $R_{ss,\ pp}$ and co-polarized transmittance $T_{ss,\ pp}$ spectra for s- and p- polarized lights at different incident angles (θ = 0°, 30°, 60° and 80°) at azimuthal angle ψ=0° for Al zig-zag thin films with 16 arms.

The co-remittance spectra (i.e., R_{ss} and T_{ss}) for the Al zig-zag film with different number of arms (4, 8, 16) at the azimuthal angle 0° and incident light angle 60° for the light with s- polarized light are shown in the Fig. 6. Since no Bragg phenomenon was observed for the Al zig-zag film with two arms, it was discarded. Also, at the incident light angle 60°, the Bragg peaks can be seen, clearly. The calculations were obtained for angle 60°, as it is close to the Brewster angle.

Since the Bragg peak depends on the period of structure, refractive index of the environment and incident light angle [39], in Al zig-zag film with 4, 8 and 16 arms there are 1, 2 and 3 Bragg peak, respectively, as shown in the Fig. 6a. Accordingly, the structure period of Al zig-zag film is equal to four arms, and so for any 4 arms, a Bragg peak is created. Also, as the number of arms increases, the intensity of the peaks created in the reflectance spectrum remains constant and only the number of reflectance spectrum peaks increases. This behavior does not see in the homogeneous and isotropic thin films. This is consistent with the results of Vepachedu et al. [32]. They showed that the Bragg phenomenon is formed in Chevronic and zig-zag (Bragg mirror) sculptured thin film of ZnSe for N=10 and N=30 unit cells at some incident light angles.

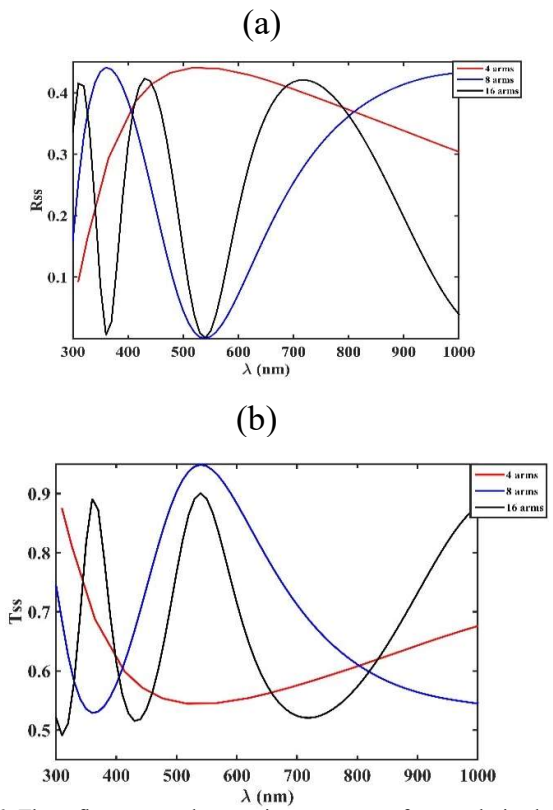

Figure 6. The reflectance and transmittance spectra for s- polarized light at incident light angle θ = 60° and azimuthal angle ψ=0° for Al zig-zag thin films with different number of arms.

3.2 Effects of arm lengths

Figure 7 shows the co-polarized reflectance $R_{ss,\,pp}$ (Fig. 7a and 7b) and co-polarized transmittance $T_{ss,\,pp}$ spectra (Fig. 7c and 7d) for both s and p- polarized light with the incident light angle θ = 60° and azimuthal angle ψ=0° for Al zig-zag thin films with 8 arms of different lengths (l=30, 60, 90, 120 nm).

For p- polarized incident light, as the length of arms increases from 30 nm to 120 nm, no changes were observed in the reflectance spectrum behavior. The co-polarized reflectance spectrum (R_{pp}) was significantly reduced for $\lambda\rangle 600\,nm$. As the length of arms increases, the transmittance spectrum decreases. So, for Al zig-zag thin films with 8 arms and length of 120 nm, transmittance spectrum tends to zero. This may be devoted to increase in the layer thickness. Therefore, the p-polarized incident light almost is absorbed by the structure.

The Bragg peaks created in reflectance spectrum of s -polarizations incident light for the zig-zag nanostructure with 8 arms and different arm lengths are given in Table 1. The red and blue shifts are shown with the arrows. For the s -polarization incident light, the number of the Bragg peaks increase as the length of arm increases from 30 nm to 120 nm. At the length of arm l = 30 nm, two peaks can be observed for $\lambda\rangle 364\,nm$ and $\lambda\sim 1000\,nm$. By increasing the arm length from 30 nm to 60 nm, two peaks are observed at $\lambda = 442\,nm$ and $\lambda = 792\,nm$, and simultaneously a peak begins to appear at $\lambda\sim 300\,nm$. Moreover, as the length of arm increases, the peak formed at low (long) wavelengths has red (blue) shift.

Simultaneously with increasing the arm length from 60 nm to 90 nm, three peaks are observed at $\lambda = 364\,nm$, $\lambda = 450\,nm$ and $\lambda = 650\,nm$. Besides, two peaks begin to appear in λ<300 nm and λ>1000 nm. Moreover, with increasing the length of arm from 60 nm to 90 nm, the peaks formed in $\lambda\langle 300\,nm$ and $\lambda = 442\,nm$ have red shift to $\lambda = 364\,nm$ and $\lambda = 450\,nm$ respectively and the peak formed at $\lambda = 792\,nm$ has blue shift to $\lambda = 650\,nm$.

Also, with increasing the length of arm from 90 nm to 120 nm, the peaks formed in $\lambda\langle 300\,nm$, $\lambda = 364\,nm$ and $\lambda = 450\,nm$ have red shift to $\lambda = 326nm$, $\lambda = 413\,nm$ and $\lambda = 476\,nm$, respectively while the peaks formed at $\lambda = 650\,nm$ and $\lambda\rangle 1000\,nm$ have blue shift to $\lambda = 619\,nm$ and $\lambda = 885\,nm$, respectively. It may be concluded that in the wavelength about $\lambda = 550\,nm$, the wavelengths are divided into two groups similar to that seen in the spectrum of T_{ss} and R_{ss}.

As the length of arm increases, the peaks formed in the wavelengths shorter (longer) than 550 nm have red (blue) shift, respectively. Also, the number of peaks increase for λ <300 nm and λ> 1000 nm. These behaviors can be seen for the nanostructures with 16 arms. But, because of the large number of peaks, their images are not shown. As a result, these nanostructures can be engineered by controlling the arm number and length and also incident light angle. Siabi et al. [40] showed that as the angle between the incident light electric field and the axis of the nano-rod increases or the length of arm decreases, the peak of the spectrum shifts to shorter wavelengths.

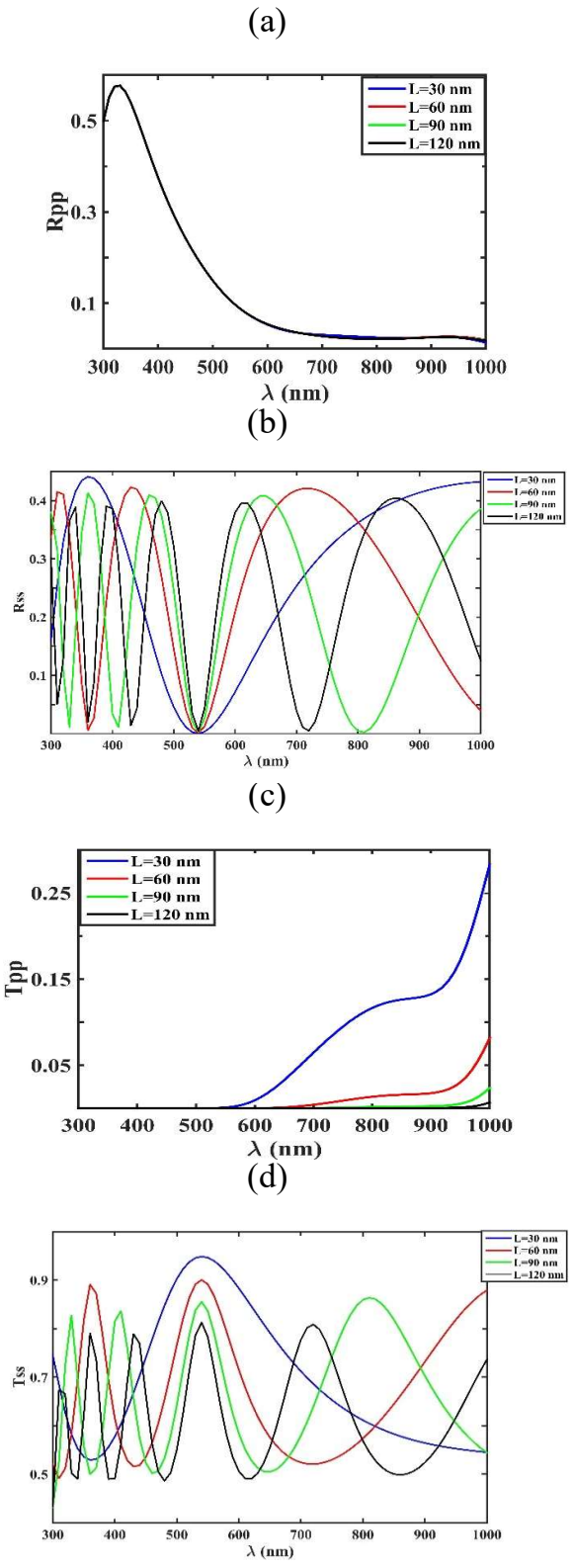

Figure 7. Co-polarized reflectance $R_{ss,\,pp}$ and transmittance $T_{ss,\,pp}$ spectra of both s- and p- polarized lights at θ = 60° angle and azimuthal angle ψ=0° for Al zig-zag thin films with 8 arms and different lengths.

Table 1. The Bragg peaks created for s- polarized incident light for Al zig-zag thin films with 8 arms of different lengths.

L (nm)	λ_{Br} (nm)							
30	364	-	-	-	-	-	-	~1000
60	~300	442	-	-	-	-	792	-
90	< 300	364	450	-	-	650	> 1000	-
120	-	326	413	476	679	885	-	-

4. Conclusions

The transfer matrix method was applied to model the reflection and transmission co-polarization spectra of zig-zag aluminum thin films by different arm numbers and lengths. The optical spectra of the zig-zag nanostructures for both s- and p- polarized lights were obtained at different incident angles. According to the results, for the s- polarized incident light, the transmission reduces and the reflection increases by incident angle. For the p- polarized light, the reflection reduces for the incident directions near the Brewster angle and the transmission almost remains constant. The numbers of Bragg peaks via arm number were also considered for s-polarized light at the 60° incident angle. The results showed four arms as the period of zig-zag structure. Besides, the red and blue shifts were observed for the wavelengths smaller and greater than 550 nm, respectively. At last, no Bragg peak was observed for p-polarized light at all incident angles.

References

[1] S. B. Mansoor and B. S. Yilbas, "Phonon transport in a curved aluminum thin film due to laser short pulse irradiation." Optics & Laser Technology, **101** (2018) 107.

[2] R. M. Pinto et al, "Piezoelectric aluminum nitride thin-films: A review of wet and dry etching techniques." Microelectronic Engineering, **257** (2022) 111753.

[3] A. K. Saikumar et al, "A review of recent developments in aluminum gallium oxide thin films and devices." Critical Reviews in Solid State and Materials Sciences, **47** (2022) 538.

[4] S. C. Lin et al, "Fabrication of Aluminum Oxide Thin-Film Devices Based on Atomic Layer

Deposition and Pulsed Discrete Feed Method." Micromachines, **14** (2023) 279.

[5] D. Ha et al, "Paper in electronic and optoelectronic devices." Advanced electronic materials, **4** (2018) 1700593.

[6] D. Nieto et al, "Aluminum thin film enhanced IR nanosecond laser-induced frontside etching of transparent materials." Optics and Lasers in Engineering, **88** (2017) 233.

[7] G. S. Rohrer et al, "The grain boundary character distribution of highly twinned nanocrystalline thin film aluminum compared to bulk microcrystalline aluminum." Journal of Materials Science, **52** (2017) 9819.

[8] A. H. Elsheikh et al., "Thin film technology for solar steam generation: A new dawn." Solar Energy, **177** (2019) 561.

[8] C. S. Oh et al., Proceedings of the 13th International Conference on Experimental Mechanics, Alexandroupolis, Greece, Springer: Berlin, Germany, (2007) pp1-6.

[9] G. Kaune et al., "Growth and morphology of sputtered aluminum thin films on P3HT surfaces." ACS applied materials & interfaces, **3** (2011) 1055.

[10] X. Yu-Qing, "Characteristics and properties of metal aluminum thin films prepared by electron cyclotron resonance plasma-assisted atomic layer deposition technology." Chinese Physics B, **21** (2012) 78.

[11] A. Ziashahabi and R. Poursalehi, "Optical Properties of Al@ Al_2O_3 Nanorod as a UV and Visible Wavelengths Plasmonic Nanostructure." Materials Science, **11** (2015) 743.

[12] R. El Beainou et al., "Electrical resistivity and elastic wave propagation anisotropy in glancing angle deposited tungsten and gold thin films." Applied Surface Science, **475** (2019) 606.

[13] M. Fakharpour "The effect of slope and number of arms on the structural properties of square tower-like manganese thin films." Journal of Nanoanalysis, **8** (2021) 7.

[14] M. Postolache et al., "Birefringence of Thin Uniaxial Polymer Films Estimated Using the Light Polarization Ellipse." Polymers, **14** (2022) 1063.

[15] G. Zhou et al., "The strain induced magnetic and anisotropic variations of lacoo3 thin films." Journal of Magnetism and Magnetic Materials, **515** (2020) 167303.

[16] F. C. Akkari et al, "Impedance spectroscopy characterization of anisotropic nano-sculptured copper oxide Cu2O thin films for optoelectronic applications." Semiconductor Science and Technology, **34** (2019) 075026.

[17] J. S. Hsu et al, "Optical polarization measurement for measuring deflection radius of the optically anisotropic flexible-polymeric substrate." Polymer Testing, **84** (2020) 106376.

[18] Y. H. Liao et al., "Antireflection of optical anisotropic dielectric metasurfaces." Scientific Reports, **13** (2023) 1641.

[19] K. Ratra, et al., "Design and analysis of omnidirectional solar spectrum reflector using one-dimensional photonic crystal." Journal of Nanophotonics, **14** (2020) 026005.

[20] A. Lakhtakia R. Messier, Sculptured thin films: Nanoengineered Morphology and Optics Vol. **143**, Bellingham, SPIE press, USA, 2005.

[21] N. Tarjányi and D. Káčik, "Birefringence of magnetic fluid thin film induced by lateral magnetic field." In AIP Conference Proceedings, **2411** (2021) 040011.

[22] T. Tanaka et al, "Nanostructure-enhanced infrared spectroscopy." Nanophotonics, **11** (2022) 2541.

[23] S. Z. Rahchamani et al, "Study of structural and optical properties of ZnS zigzag nanostructured thin films." Applied Surface Science, **356** (2015) 1096.

[24] S. Z. Rahchamani et al, "Anisotropic optical properties of ZnS thin films with zigzag structure." Bulletin of Materials Science, **40** (2017) 897.

[25] Susann Liedtke et al, "Comparative study of sculptured metallic thin films deposited by oblique angle deposition at different temperatures." Beilstein journal of nanotechnology, **9** (2018) 954.

[26] M. G. Arashti and M. Fakharpour, "Fabrication and characterization of Al/glass zig-zag thin film, comparing to the discrete dipole approximation results." The European Physical Journal B, **93** (2020) 1.

[27] M. Fakharpour et al., "Electrical characterization of zig-zag Aluminum thin films using experimental and theoretical methods." Journal of Optoelectronical Nanostructures, **6** (2021) 25.

[28] S. A. Jewell et al., "Circularly polarized colour reflection from helicoidal structures in the beetle Plusiotis boucardi." New Journal of Physics, **9** (2007) 99.

[29] P. Vukusic et al, "A biological sub-micron thickness optical broadband reflector characterized using both light and microwaves." Journal of the Royal Society Interface, **6** (2009) 193.

[30] J. A. Sherwin et al, "Homogenization of similarly oriented, metallic, ellipsoidal inclusions using the Bruggeman formalism." Optics communications, **178** (2000) 267.

[31] A. Lakhtakia and Mod. Simul, "Axial loading of a chiral sculptured thin film." Modelling and Simulation in Materials Science and Engineering, **8** (2000) 677.

[32] V. Vepachedu et al, "Nonexhibition of Bragg phenomenon by chevronic sculptured thin films: experiment and theory." Journal of Nanophotonics, **11** (2017) 036018.

[33] J. A. Sherwin, A. Lakhtakia, I. J. Hodgkinson, "On calibration of a nominal structure–property relationship model for chiral sculptured thin films by axial transmittance measurements." Optics communications, **209** (2002) 369.

[34] E. D. Palik, Handbook of optical constants of solids. Academic press, New York, Vol .3, (1998).

[35] M. Fakharpour et al., "Engineering Mn as tetragonal-like helical sculptured thin film for broadband absorption." Plasmonics, **11** (2016) 1579.

[36] F. Babaei and H. Savaloni, "Reflection, transmission and circular dichroism in axially excited slab of a copper thin film helicoidal bianisotropic medium." Optical Communication, **278** (2007) 321.

[37] B, Dick et al., "Controlled growth of periodic pillars by glancing angle deposition." Journal of Vacuum Science & Technology B: Microelectronics and Nanometer Structures Processing, Measurement, and Phenomena, **21** (2003) 23.

[38] K. M. McPeak et al., "Plasmonic films can easily be better." rules and recipes. ACS photonics, **2** (2015) 326.

[39] S. V. Kesapragada et al., "Nanospring pressure sensors grown by glancing angle deposition." Nano letters, **6** (2006) 854.

[40] A. Siabi-Garjan, and H. Savaloni, "Extinction spectra and electric near-field distribution of Mn nano-rod based sculptured thin films: experimental and discrete dipole approximation results." Plasmonics, **10** (2015) 861.